Materials Horizons

ROYAL SOCIETY OF CHEMISTRY

COMMUNICATION

View Article Online
View Journal | View Issue

Cite this: *Mater. Horiz.*, 2025, **12**, 3408

Received 4th December 2024,
Accepted 5th February 2025

DOI: 10.1039/d4mh01753f

rsc.li/materials-horizons

Machine-learning accelerated prediction of two-dimensional conventional superconductors†

Thalis H. B. da Silva,[a] Théo Cavignac,[b] Tiago F. T. Cerqueira,[a] Hai-Chen Wang[b] and Miguel A. L. Marques*[b]

We perform a large scale search for two-dimensional (2D) superconductors, by using electron–phonon calculations with density-functional perturbation theory combined with machine learning models. In total, we screened over 140 000 2D compounds from the Alexandria database. Our high-throughput approach revealed a multitude of 2D superconductors with diverse chemistries and crystal structures. Moreover, we find that 2D materials generally exhibit stronger electron–phonon coupling than their 3D counterparts, although their average phonon frequencies are lower, leading to an overall lower T_c. In spite of this, we discovered several out-of-distribution materials with relatively high-T_c. In total, 105 2D systems were found with $T_c > 5$ K. Some interesting compounds, such as CuH_2, NbN, and V_2NS_2, demonstrate high T_c values and good thermodynamic stability, making them strong candidates for experimental synthesis and practical applications. Our findings highlight the critical role of computational databases and machine learning in accelerating the discovery of novel superconductors.

New concepts

This study introduces a large-scale computational approach to discover two-dimensional (2D) superconductors by combining density-functional perturbation theory (DFPT) with machine learning models. Unlike existing research, which often focuses on smaller datasets or specific material types, our work screens over 140 000 2D compounds from the Alexandria database, revealing numerous 2D superconductors with diverse chemistries and crystal structures. A key differentiation is the finding that 2D materials exhibit stronger electron–phonon coupling compared to their 3D counterparts, although lower average phonon frequencies result in generally reduced critical temperatures (T_c). Despite this, we identified several out-of-distribution materials with relatively high T_c, including CuH_2, NbN, and V_2NS_2, which also show good thermodynamic stability. This approach highlights the potential of leveraging computational databases and machine learning to accelerate the discovery of superconductors, offering a pathway to identify experimentally realizable materials with promising properties for practical applications.

I. Introduction

The discovery of superconductivity in 2D materials[1–4] has opened up new possibilities for ultra-thin and flexible superconducting devices, essential for applications such as compact magnetic field sensors, efficient power transmission lines, and advanced quantum technologies. These materials can significantly enhance the performance of superconducting qubits, which are vital for quantum computing, owing to their stability and fault tolerance.[5,6] Moreover, their high current density can lead to improved efficiency in power transmission systems, high-field magnets, and nanoscale radiation detectors[7].

Superconductivity in a variety of 2D transition metal dichalcogenides has been measured experimentally.[8–13] In these systems, charge density wave[10,14,15] and Ising pairing[16–18] can coexist with the condensation of Cooper pairs.[19,20] The competition and cooperation between these states forms an intriguing physical picture, for which numerous efforts have been made to give insights from the theoretical point of view.[14,21–29] Superconductivity was also discovered in twisted bilayer graphite at low twisting angles,[30,31] although at rather low transition temperature (T_c).

In conjunction with these advancements, numerous theoretical investigations have examined (hypothetical) 2D materials as potential conventional superconductors.[19] Already in 2014 it was predicted that heavy electron doping could turn graphene into a superconductor.[32] Density functional theory (DFT) calculations also showed that monolayer LiC_6 and CaC_6 could have a T_c of 8.1 K and 1.4 K.[33] Moreover, strained monolayer LiC_{12} and AlC_8 could become high T_c superconductors, reaching 20.3 K[34]

[a] *CFisUC, Department of Physics, University of Coimbra, Rua Larga, 3004-516 Coimbra, Portugal*
[b] *Research Center Future Energy Materials and Systems of the University Alliance Ruhr and Interdisciplinary Centre for Advanced Materials Simulation, Ruhr University Bochum, Universitätsstraße 150, D-44801 Bochum, Germany. E-mail: miguel.marques@rub.de*

† Electronic supplementary information (ESI) available. See DOI: https://doi.org/10.1039/d4mh01753f

and 41 K[35] under 10% and 12% strain, respectively. Li-adsorption is also predicted to convert the insulating monolayer boron nitride (h-BN) to a superconductor.[36] Other graphene-related compounds formed by different ration of squares, hexagons, and octagons could also become superconductors. Notably, octagraphene[37,38] and biphenylene[39] are predicted to become conventional superconductors below 20.8 K[40] and 3.02 K,[39] respectively. Another interesting 2D compound is the fully hydrogenated form of graphene, the so-called graphane (CH),[41,42] where all C-atoms are bonded to four neighbors (one hydrogen and three carbons). Although full hydrogenation of graphene is hardly achievable so far,[43,44] graphane still attracts great interest due to its high predicted T_c = 90 K.[45] Various other "Xenes", *i.e.* two-dimensional elementary structures (not limited to the honeycomb lattice), have been predicted to show superconductivity under electron or hole doping, namely, leadene,[46] silicene,[47] phosphorene,[48] arsenene,[49] aluminene,[50] gallenene,[51] as well as antimonene.[52]

Due to the high T_c of three dimensional MgB_2, that is driven by the in-plane stretching phonons of boron 2D layers, boron has attracted greater interest than any other element in the search for 2D superconductors. Borophene has a T_c as high as 24.7 K if vacancies are formed in stripes[53]. Similarly, multiple 2D boron allotropes predicted from evolutionary algorithms have T_c ranging from 6.7 K to 27.6 K.[54,55] Furthermore, doping with Sr was predicted to increase T_c of the boron Kagome monolayer up to 20.9 K.[56] Also several borides, where boron is combined with metallic elements, have been studied. Metals that were predicted to lead to superconductivity are alkaline-earth or Li,[57–59] group III metals[60,61] and transition metals.[58,62–65] Interestingly, ferromagnetic 2D Mn-borides are predicted to be electron–phonon superconductors.[66,67] Other boron related 2D compounds that are also predicted as conventional superconductors are hydrogenated borides ($Ti_2B_2H_4$[68] and TiB_2H[69]), 2D boron carbides,[70–72] boron silicides,[73] boron chalcogenides,[74] penta-structure 2D boron nitrides,[75] and boron phosphide.[76] Another interesting boron-related 2D system is the borophene oxide B_2O that, unlike the insulating B_2O_3,[77] is metallic and superconducting, with a T_c relatively high (10.3 K) comparing to other 2D borides.[78]

Theoretical studies have also predicted several other 2D superconducting compounds, *e.g.* nitrides,[79] silicides,[80] metal silicon nitrides,[81] phosphorus carbide,[27] 2D metal–organic frameworks (2D-MOFs),[82] and MXenes.[83–86] Unlike the other 2D-families, in MXenes the surface functional groups play an important role for superconductivity.[83,87–89]

As we see, the theoretical search for new 2D superconductors has been very fruitful in the past decade. However, most of the searches rely on physical intuition and usually focus on a few structure prototypes and chemical elements. In such a way, the theoretical exploration of unknown chemical and structural spaces is limited. Fortunately, recently developed computational databases[90–96] and machine learning methodologies,[97] enable a different approach to discover superconducting materials. Several high-throughput searches on three-dimensional (3D) inorganic conventional superconductors have been conducted,[98–101] unveiling thousands of potentially superconductors, some of them with potentially record T_c.[102,103] Moreover, the models and workflow designed originally for the 3D worlds can be easily extended to 2D cases. This was already exemplified in ref. 104, where over 1000 2D structures from the JARVIS-DFT database[105] were screened. In total, 34 dynamically stable structures with $T_c > 5$ K were identified, including materials such as W_2N_3, NbO_2, ZrBrO, TiClO, $NaSn_2S_4$, $Mg_2B_4C_2$, and $Mg_2B_4N_3$, with T_c reaching as high as 21.8 K.

In this work, we take a step further by developing a large and accurate dataset of calculated electron–phonon and superconducting properties for 2D materials. This dataset is then used to train a reliable machine-learning model for predicting the transition temperature T_c of 2D superconductors. This model was then utilized to screen for superconductivity the 2D compounds present in the Alexandria[96] database, that includes more than 140 000 entries, unveiling numerous systems with interesting superconducting properties.

II. Results and discussions

A. Initial dataset

The first step in this work is the creation of an (unbiased) dataset. The objective is twofold: (i) to be able to compare directly electron–phonon and superconducting properties of 2D materials with their 3D counterparts; (ii) to allow for the training of machine learning models to perform an accelerated high-throughput study of 2D superconductors. To construct this dataset we select 2D materials from the Alexandria database,[96] choosing (*meta*-)stable ones with an energy above the convex hull (E_{hull}) of less than 250 meV per atom. To decrease the numerical cost, we discard compounds with a layer space group number of lower than 30. Furthermore, we restrict the search only to metallic materials by removing materials with a density of states at the Fermi level less than 0.1 states per eV (per unit cell). Finally, we only consider structures with up to 8 atoms in the unit cell. This initial dataset comprises 4383 compounds, belonging to a large diversity of chemical systems, space groups, and structural arrangements.

The next step is the calculation of the phonon spectrum and electron–phonon coupling within the framework of density functional perturbation theory (DFPT), as detailed in III. It turns out that the majority of the compounds studied exhibited imaginary frequencies in the Brillouin zone. We have found a similar situation for metastable 3D systems with distances to the convex hull comparable to the ones of the 2D systems studied here. Ultimately, this is a consequence of the symmetry-preserving prototype search used to build modern large material databases. For the ~900 dynamically stable materials, we calculated the superconducting critical temperature (T_c) using the Allen–Dynes modification[106] to the McMillan formula[107,108] (see III).

In the top panel of Fig. 1 we show a periodic table indicating the number of occurrences of each element present in the initial dataset. We can see that almost the entire periodic table is well represented although with a larger weight towards systems with halogens, chalcogens and pnictogens. This can

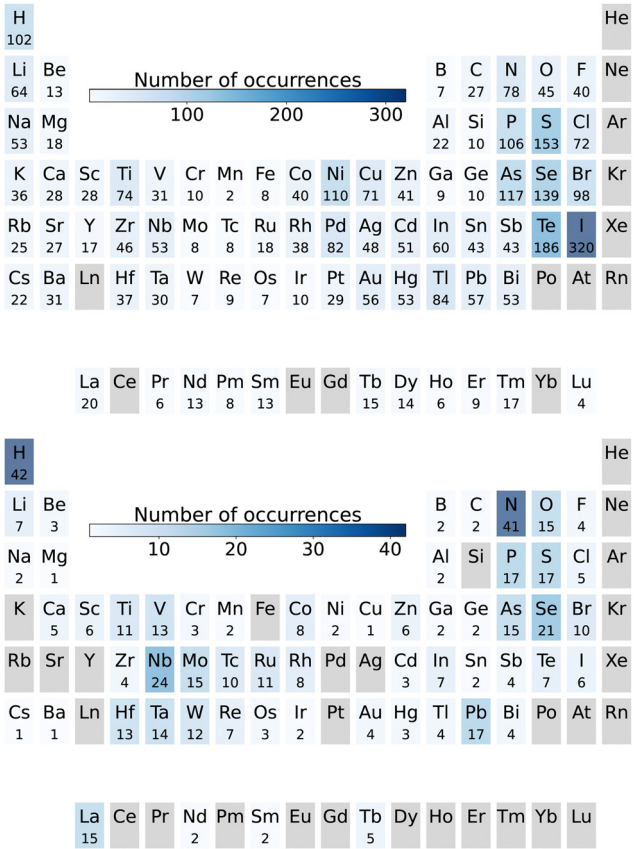

Fig. 1 Top: Number of occurrences of a given chemical element in the training data set; bottom: number of occurrences of a given chemical element for all 2D superconductors found with $T_c > 5$ K.

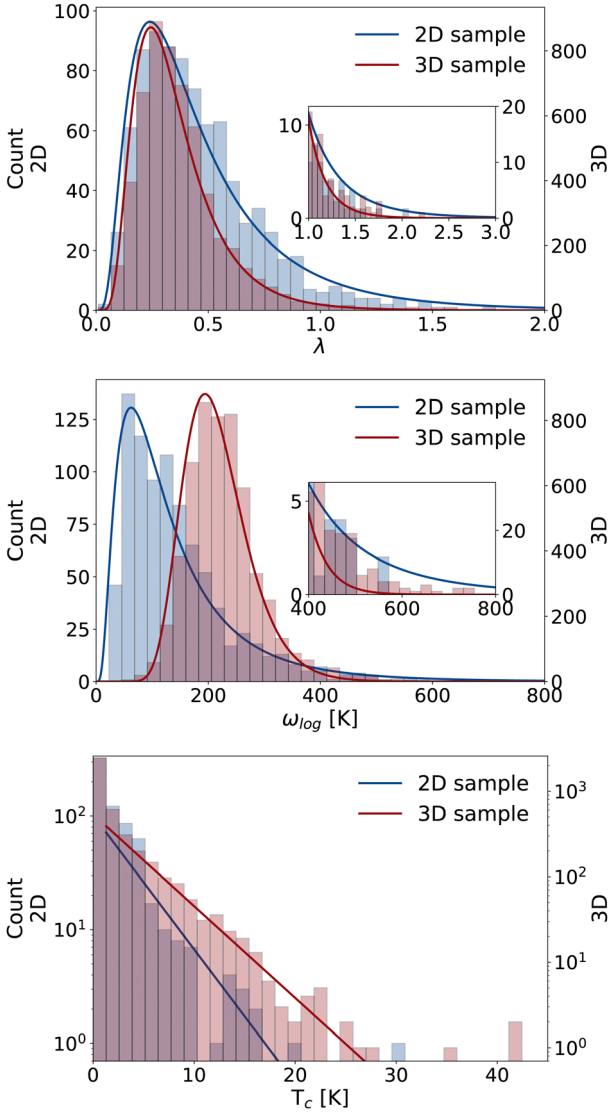

Fig. 2 (a) Histogram of the electron–phonon coupling constant λ. The blue and red lines are fits to a log-normal distribution with parameters $\sigma^{2D} = 0.6884$, $\mu^{2D} = -0.9532$, $N^{2D} = 50.59$, and $\sigma^{3D} = 0.5058$, $\mu^{3D} = -1.157$, $N^{3D} = 306.2$; (b) histogram of the logarithmic averaged phonon frequency ω_{log}. The blue and red lines are fits to a log-normal distribution with parameters $\sigma^{2D} = 0.7479$, $\mu^{2D} = 4.692$, $N^{2D} = 2.020 \times 10^4$, and $\sigma^{3D} = 0.2714$, $\mu^{3D} = 5.342$, and $N^{3D} = 1.206 \times 10^5$; (c) histogram of the values of the transition temperature T_c. Note the logarithmic scale on the y-axis. The blue and red lines are fits to an exponentially decaying distribution ($\rho(x) = N\kappa e^{-\kappa x}$) with parameters $\kappa^{2D} = 0.2717$, $N^{2D} = 374.4$, and $\kappa^{3D} = 0.2473$, $N^{3D} = 2172$. All fits were performed using scipy.[109] The number of bins in the distributions was set to 35.

be understood by noticing that in addition to the selection criteria indicated above, there is a bias related to the database. In fact, a large number of the 2D compounds present in Alexandria were obtained through a systematic procedure that imposed charge neutrality, naturally generating compounds with non-metals. Interestingly, the most frequent element in the whole set is iodine, probably due to the I^{-1} oxidation state that is compatible with many stoichiometries, and its relatively small electronegativity (when compared to other non-metals) that lead to compounds with a larger probability of being metallic. On the other hand, the most frequent metallic element is nickel, which usually forms magnetic compounds that are not superconducting.

In Fig. 2 we show the distribution of key superconducting properties, including the electron–phonon coupling constant (λ), the logarithmic average of the phonon frequencies (ω_{log}), and the T_c calculated with the Allen–Dynes formula (see III). To shed some light on the difference between 2D and 3D, we plotted also the histogram from our previous search of 3D compounds.[101]

First we can notice that the number of compounds in the 2D set is large enough to lead to similar smooth distributions as in the 3D case. The λ distribution shows a higher proportion of systems with stronger electron–phonon coupling in 2D, with the average λ going from 0.357 in 3D to 0.489 in 2D. This is true, even if the 2D systems generally have much smaller Fermi surfaces. Furthermore, as the position of the peak is close in the two cases, we can still expect that the mechanism that leads to electron–phonon coupling in most 2D materials is similar to 3D, in spite of the different bonding patterns and atomic coordinations. The most visible difference is observed in the ω_{log} histogram, with the average ω_{log} for 2D materials being 144 K, around 70 K lower than in 3D. Both the average increase of λ and the decrease of ω_{log} can be understood by noticing that

out-of-plane modes in 2D materials are not constrained by the presence of atoms, leading to lower phonon frequencies for these modes. Of course, this softening can, in some cases, also lead to imaginary phonons. Finally, the distribution of T_c can be well fit with an exponentially decaying distribution, although we do find some outlier compounds with higher values of T_c. When comparing to the 3D case, we find that the red-shift of the distribution of T_c leads to a faster decay in 2D. This seems to indicate that, on average, the decrease of dimensionality hinders conventional superconductivity in spite of the increase of the electron–phonon coupling.

B. Machine-learning accelerated search

Despite the specificity of 2D systems, much of the chemistry and the physics relevant for conventional superconductivity is shared with 3D bulk compounds. As such, we decided to combine our 2D data with the results for 3D systems from ref. 101 and to use this larger dataset to train a machine learning model that predicts T_c from a structure, as described in III. This strategy allows to obtain reasonable errors for the machine learning prediction of the superconducting properties of 2D systems already with the relatively small initial 2D dataset.

We used this machine to predict T_c for all 2D compounds in the Alexandria database that were metallic, had a maximum of 12 atoms in the unit cell, and a layer space group number greater or equal to 15. Next, we calculated the electron–phonon and superconducting properties for the 2365 structures that the machine predicted with a $T_c > 5$ K. Not surprisingly, many of these compounds (2037) exhibited imaginary frequencies and were discarded.

A periodic table summarizing the chemistry of all superconductors (both from the initial dataset and materials proposed by the machine) with T_c greater than 5 K is shown in the lower panel of Fig. 1. Notably, the observed patterns differ significantly from those in the initial dataset (upper panel). Hydrogen, as expected in high-T_c compounds, is the most frequently occurring element, followed by nitrogen and niobium. However, when compared to their 3D counterparts,[101] 2D superconductors exhibit a much greater diversity in chemical composition. We also note the presence of several heavy chemical elements, such as Hf, Ta, W, Pb, or even La.

Table 1 Top 10 compounds discovered in this work ranked by T_c (in K), with their electron–phonon coupling constants (λ), logarithmically averaged phonon frequencies (ω_{log} in K), the distance from the convex hull of stability (E_{hull} in eV per atom) as well as the reference number of each compound in the SI

Formula	λ	ω_{log} (K)	T_c^{AD} (K)	E_{hull}	
CuH_2	1.05	376	30.4	0.173	SI #64
NbN	1.55	177	24.1	0.307	SI #37
W_2N_3	1.49	184	24.0	0.339	SI #5
Ti_2O_3	0.96	317	22.1	0.285	SI #8
RhO_2	1.26	197	20.9	0.158	SI #68
Nb_2CO_2	1.09	237	20.2	0.124	SI #83
Ru_2O_3	1.54	127	17.2	0.454	SI #15
Tc_4H_3	1.02	221	17.0	0.417	SI #19
VH_3	0.87	271	16.0	0.157	SI #69
ReH_2	0.95	231	15.9	0.480	SI #65

C. Example compounds

Finally, we performed more accurate calculations for all compounds discovered in our high-throughput approach with $T_c > 5$ K (see III). In this process we encountered some unstable compounds, typically with imaginary frequencies at low-symmetry q-points (probably due to charge density wave instabilities). A complete list of the 105 dynamically stable 2D superconductors we found with $T_c > 5$ K, including the crystal structure, electronic structure, phonon band structure and Eliashberg spectral function, can be found in the ESI.† Furthermore, we include a unique identifier that we use to reference the compounds in the following. In Table 1 we highlight the top 10 dynamically stable superconductors with the highest T_c.

At the top of the list we find CuH_2 (SI #64). It is not surprising to find a hydride at the top of our list, as it is well-known that due to the very light mass of hydrogen these compounds are expected to be able to yield high-T_c.[110,111] In fact, we find other hydrides with rather high values for the transition temperature, such as Tc_4H_3 (SI #19) with $T_c = 17.0$ K, or VH_3 (SI #69) with $T_c = 16.0$ K. At the top of the list we also find several nitride compounds (*e.g.* NbN) and oxides (*e.g.* Ti_2O_3).

CuH_2 crystallizes in a structure with $p$mmn symmetry (layer space group #46) with all atoms in the Wyckoff 2b position (see Fig. 3(a)). The Cu atoms form a buckled triangular layer, with the H above and below the Cu-layer. This material has a relatively simple electronic band structure, with only two bands with Cu–H hybrid character crossing the Fermi energy. Furthermore, these two bands are degenerate in several symmetry lines, and are highly dispersive in large parts of the Brillouin zone. Below these bands, we find the manifold of fully occupied Cu-d bands in the range from −5 to −2 eV. The acoustic phonon modes and the three lowest lying optical modes have Cu-character, as expected due to the large mass of Cu relatively to H. The remaining, higher-energy modes, with H-character, are divided in three separate manifolds. The largest contribution to the electron–phonon coupling constant comes from the Cu- and lowest lying H-modes, leading to a reasonably large $\lambda = 1.05$. However, the highest-lying H-modes contribute significantly to the value of $\omega_{log} = 376$ K, resulting in $T_c = 30.4$ K. CuH_2 is 0.173 eV per atom above the convex hull of stability, decomposing into elemental Cu and H_2. This value is not particularly high, especially when compared with 2D compounds that have been synthesized like silicene (0.640 eV per atom above the hull[93]) or germanene (0.482 eV per atom above the hull[93]), but indicates that the interaction with a suitable substrate will be required for its stabilization and experimental synthesis. We found that the Pd (110) surface has a minimal 0.02% lattice mismatch with CuH_2, and therefore is a good candidate for the synthesis of this 2D compound.

The structure of NbN (see SI #37), the compound with the second highest T_c in Table 1, features a thick sheet composed of four layers (see Fig. 3(b)). In each of the layers, the NbN atoms form a slightly buckled square lattice. The layers are stacked such that the Nb in one layer is on top of N in the neighboring layers. This compound crystallizes in layer group $p4$/nmm (#64) with 8 atoms in the primitive unit cell, all in the Wyckoff 2b position. The electronic band structure of this compound is rather complex, with many bands – arising from

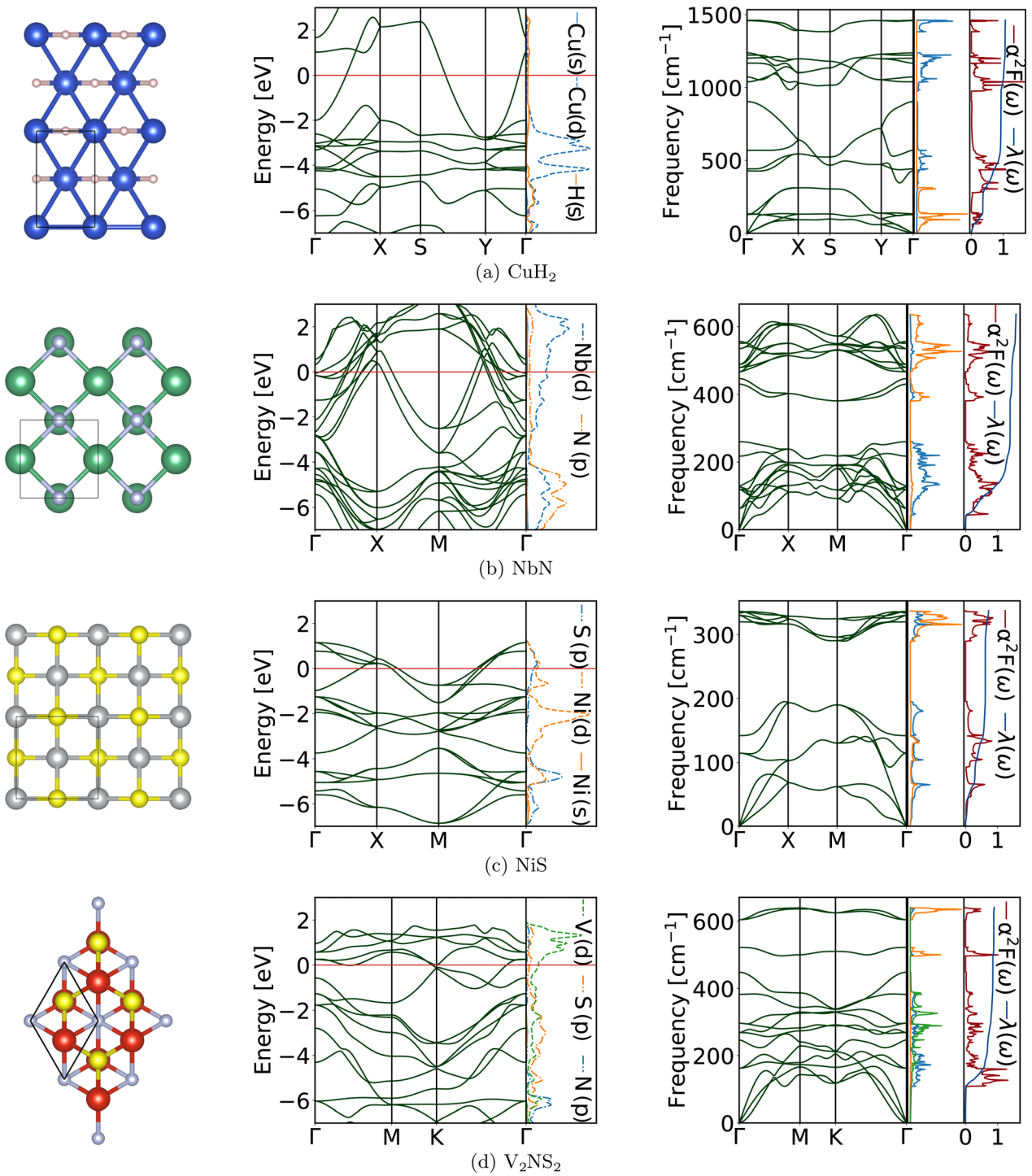

Fig. 3 Example 2D superconductors found in this work. The columns represent the chemical composition, a depiction of the crystal structure seen from the direction of the aperiodic axis, the electronic band structure and density of electronic states, and the phonon band structure, density of phonon states, and Eliashberg spectral function $\alpha^2F(\omega)$. In (a), Cu atoms are in blue and H in white; in (b), Nb atoms are in dark green and N in gray; in (c), Si atoms are in yellow and N in gray; in (d), V atoms are in red, N in gray and S in yellow. The primitive unit cell is also indicated.

the symmetry breaking due to the presence of the four layers – that cross the Fermi energy, leading to a very complicated Fermi surface. The phonons are well separated in two groups due to the very different masses of N and Nb. Most of the value of λ arises from the very strong coupling of the acoustic and low-lying optical modes that have mostly Nb character. This leads to the very large λ = 1.56 but a relatively modest $\omega_{\log}$ = 177 K, resulting in a T_c of 24.1 K. The energy above hull of 0.307 eV per atom indicates moderate thermodynamic stability, suggesting that NbN might be difficult to synthesize experimentally,

although it might be stabilized by a surface such as Pd (110) that has a very small lattice mismatch of 0.49%. We note that NbN together with Tc_4H_3 (SI #19) are the thickest compounds present in Table 1. We found several other multilayer structures with $T_c > 5$ K, including NbC (SI #43), that forms a three-layer sheet with alternating Nb and C atoms, and ScO (SI #44), that exhibits a similar configuration with alternating Sc and O atoms.

As an example of a chalcogenide superconductor, we show NiS in Fig. 3(c). This compound features a distinctive layered arrangement, where the atoms are organized in a square lattice, with S atoms alternating between the top and bottom of a Ni layer. This configuration results in a characteristic zigzag pattern when viewed from the side, a motif commonly observed in superconductors in this study, for example TiS (SI #41), TaTe (SI #42), CrRu (SI #48), and Co_2TeSe (SI #104), as well as others listed in the SI. NiS crystallizes in the tetragonal space group $p4/nmm$ (#64) with 4 atoms in the primitive unit cell, where Ni and S atoms occupy the 2a and 2b Wyckoff positions, respectively. The band structure of NiS exhibits a Ni–S hybrid character in the bands above the Fermi level, transitioning to a predominantly Ni character below the Fermi energy until approximately −4 eV, where a significant contribution coming from the S-2p orbitals emerges. Phonon analysis reveals that the acoustic modes and the lowest optical mode have an overall hybrid character, with a slightly larger Ni contribution. As the frequency increases, the next two modes become predominantly Ni-driven, while the highest modes are dominated by S, which is expected due to the lower mass of S compared to Ni. The relatively broad dispersion of the lowest modes and the tightly grouped high-frequency modes contribute to an average electron–phonon coupling constant of $\lambda = 0.71$ and a logarithmic average phonon frequency of $\omega_{log} = 142$ K resulting in a superconducting critical temperature of $T_c = 5.8$ K. A calculation including anisotropy shows that NiS has multiple superconducting gaps, which is not surprising in view of the three bands crossing the Fermi surface. However, this does not affect the transition temperature significantly, with T_c remaining below 6 K. This material is only 0.100 eV per atom above the convex hull, indicating good thermodynamic stability. For NiS, the optimal substrate seems to be the Rh (110) surface (0.63% mismatch).

Finally, in Fig. 3(d) we show V_2NS_2, a representative of the family of 2D superconductors for which we found more compounds. This prototype (A_2BC_2) features a thick-layered structure composed of five atomic layers arranged in a sandwich-like configuration. At the center of the slab we find a layer of B-atoms (here N), surrounded on both sides by layers of A-atoms (V), which are further capped by C-atoms (S) layers. Viewed from above, the structure forms a hexagonal pattern, crystallizing in the trigonal space group $p\bar{3}m1$ (#72). The primitive unit cell contains 5 atoms, with the A and C atoms occupying the 2c Wyckoff positions while the B atom occupies the 1a Wyckoff position. In this family we identified 7 superconductors, namely Mo_2BSe_2, V_2BSe_2, Nb_2CO_2, Ta_2NS_2, V_2NS_2, Ti_2NSe_2, and Nb_2NSe_2. The highest T_c in this family belongs to Nb_2CO_2 ($T_c = 20.2$ K), however this system has larger E_{hull} (0.124 eV per atom) than V_2NS_2 that was found to be merely 0.050 eV per atom above the hull. This suggests good thermodynamic stability and a strong likelihood of being experimentally synthesizable. For V_2NS_2 we found that the Ir (110) facet is a good substrate candidate with 2.29% mismatch. The electronic band structure of V_2NS_2 features a doubly degenerate Dirac point at K and extra crossing of the Fermi surface between K and Γ. Furthermore, the Fermi level touches the conduction band between M and Γ. The lowest-energy electrons originate from both S and V, while above the Fermi level, the electrons come predominantly from V. The phonon band structure reveals a high density of medium-frequency modes, primarily stemming from vibrations of the V and S atoms. Additionally, two high-frequency modes are observed, originating from the vibrations of the inner N atoms. These high frequency N modes are expected due to the lower mass of N compared to S and V, as well as its spatial constraints. The high density of low-frequency modes contributes to an electron–phonon coupling constant of $\lambda = 0.88$, while the high-frequency modes from nitrogen contribute significantly to the value of $\omega_{log} = 246$ K, resulting in a critical transition temperature of $T_c = 14.4$ K. We note that a calculation including anisotropy reveals that V_2NS_2 is indeed a single gap superconductor, but with a slight increase of T_c to about 19 K.

D. Discussion

We showed how using machine learning models, combined with standard density-functional based methods, can be used to explore, in a very efficient manner, 2D superconductors. It turns out that in 2D the electron–phonon coupling is stronger than in 3D, but the average phonon frequency decreases, due to the lower frequency of out-of-plane modes. Even if this leads to a decrease of the average transition temperature of 2D compounds with respect to 3D compounds, we still find a number of out-of-distribution systems with considerably higher T_c. As in 3D, the presence of hydrogen, nitrogen, or niobium are advantageous for superconductivity in 2D, but we also find systems with many other chemical elements. From our workflow, several interesting compounds, emerged, not only with relatively high-T_c, but also with rather low distances to the convex hull of thermodynamic stability suggesting that they are good candidates for experimental synthesis.

In spite of these advancements, we still face a number of challenges. The training set for the machine learning models still contains a relatively small number of 2D compounds, that translates into sizeable errors in the predictions. The solution to this problem is straightforward, specifically running electron–phonon calculations for more 2D compounds, so we expect significant improvements in the near future. We note that the prediction of superconducting properties will also benefit from any advances in machine learning methods for the prediction of structure–property relationships.

Another issues arises from the fact that we have a much smaller knowledge of 2D materials, both experimentally and theoretically, than of 3D compounds. For example, there are around 140 thousand 2D compounds in Alexandria while this database contains 5 million 3D compounds. Furthermore, the large majority of the 2D compounds contain non-metallic chemical elements, leading to a reduced number of intermetallic

compounds, many of them potentially superconducting. An exploration of the 2D space, for example by using machine-learning-accelerated high-throughput searches that were extremely successful in the 3D world, is therefore a necessity to find novel 2D superconductors with interesting and unexpected properties.

III. Methods

We chose the parameters of our *ab initio* calculations in order to ensure compatibility (whenever possible) with our previous work on 3D superconductors.[101] All density-functional calculations were performed using version 7.1 of Quantum Espresso[112,113] with the Perdew–Burke–Ernzerhof functional for solids (PBEsol)[114] generalized gradient approximation. We used the PBEsol pseudopotentials[114] from the pseudodojo project,[115] specifically the stringent, scalar-relativistic norm-conserving set. Geometry optimizations were performed using uniform Γ-centered k-point grids with a density of $1.5 \times (6\pi)^2$ k-points per Å^{-2}. If this resulted in an odd number of k-points, the next even number was used instead. We ensured that a vacuum region of 15 Å separated the layers, and we truncated the Coulomb interaction in the z-direction following the method of ref. 116. Convergence thresholds for energies, forces, and stresses were set to 1×10^{-8} a.u., 1×10^{-6} a.u., and 5×10^{-2} kbar, respectively. For the electron–phonon coupling, we used a double-grid technique, with the same k-grid used in the lattice optimization as the coarse grid, and a k-grid quadrupled in each direction as the fine grid. For the q-sampling of the phonons, we used half of the k-point grid described above. For all k- and q-point samplings, we used a single point in the aperiodic direction. The double δ-integration to obtain the Eliashberg function was performed with a Methfessel–Paxton smearing of 0.05 Ry. For the higher precision calculations, we repeated the previous steps by changing the initial k-point grid density to $3 \times (6\pi)^2$ k-points per Å^2 and by setting the k-grid used as the coarse grid to double the k-grid used for the geometry optimization.

For the machine learning part, we trained the Alignn[117] model using, as targets, λ, $\omega_{\log}$, and T_c simultaneously, with the error for each property weighted equally. The dataset used contained both 3D and 2D data, and we employed a random split of 90%/5%/5% for training/validation/test sets. The mean absolute error (MAE) on the test set for the final model was 0.151, 31.9 K, and 2.51 K for λ, $\omega_{\log}$, and T_c, respectively. For reference, the mean values on the test set for λ, $\omega_{\log}$, and T_c are 0.533, 277 K, and 6.16 K. When considering only the 2D materials present in the test set, the corresponding MAEs are 0.204, 31.3 K, and 1.65 K, for mean values of 0.495, 147 K, and 1.36 K. While the error on T_c is significant, we can still see its usefulness for screening new 2D superconductors. When examining the values obtained with DFPT for the 2D materials recommended by the model, we observe that 33% of the calculated T_c values are above the 5 K threshold. This value should be compared to 13% success rate for our initial dataset.

The values of

$$\lambda = 2\int \frac{\alpha^2 F(\omega)}{\omega} \mathrm{d}\omega, \tag{1a}$$

$$\log(\omega_{\log}) = \frac{2}{\lambda}\int \frac{\log(\omega)}{\omega} \alpha^2 F(\omega) \mathrm{d}\omega, \tag{1b}$$

$$\omega_2^{\,2} = \frac{2}{\lambda}\int \omega \alpha^2 F(\omega) \mathrm{d}\omega, \tag{1c}$$

where $\alpha^2F(\omega)$ is the Eliashberg spectral function, were used to calculate the superconducting transition temperature using the Allen–Dynes modification[106] to the McMillan formula[107,108]

$$T_c^{\mathrm{McMillan}} = f_1 f_2 \frac{w_{\log}}{1.20} \exp\left[-1.04 \frac{1+\lambda}{\lambda - \mu^*(1+0.62\lambda)}\right], \tag{2}$$

where

$$f_1 = \left\{1 + \left[\frac{\lambda}{2.46(1+3.8\times\mu^*)}\right]^{3/2}\right\}^{1/3} \tag{3a}$$

$$f_2 = 1 + \frac{\lambda^2\left(\omega_2/\omega_{\log} - 1\right)}{\lambda^2 + \left[1.82(1+6.3\mu^*)\omega_2/\omega_{\log}\right]^2} \tag{3b}$$

We took arbitrarily $\mu^* = 0.10$ for all materials studied, a value that has become rather standard in this kind of studies.

Author contributions

T. H. B. S. and T. C. developed the high-throughput workflow; T. F. T. C. trained the machine learning model and performed the predictions; H.-C. W. and M. A. L. M. performed the response calculations and directed the research. All authors participated equally in the interpretation of the results and in the writing of the manuscript.

Data availability

The data produced in this work can be downloaded from the Alexandria database[96] at **https://alexandria.icams.rub.de/**. The workflow, and the model together with the dataset used for its training is available on GitHub at **https://github.com/hyllios/utils/**.

Conflicts of interest

The authors declare that they have no competing interests.

Acknowledgements

T. F. T. C. acknowledges the financial support from FCT – Fundação *para* a Ciência e Tecnologia, I.P. through the projects UIDB/04564/2020 and CEECINST/00152/2018/CP1570/CT0006, with DOI identifiers 10.54499/UIDB/04564/2020 and 10.54499/CEECINST/00152/2018/CP1570/CT0006 respectively, and computing resources provided by the project Advanced Computing Project 2023.14294.CPCA.A3, platform Deucalion. M. A. L. M. acknowledges partial funding from the Horizon Europe MSCA Doctoral network grant n.101073486, EUSpecLab, funded by the European Union. M. A. L. M. acknowledges the Keele

Foundation through the SuperC collaboration. The authors thank the Gauss Centre for Supercomputing e.V. (https://www.gauss-centre.eu) for funding this project by providing computing time on the GCS supercomputer SUPERMUC-NG at the Leibniz Supercomputing Centre (https://www.lrz.de) under the project pn25co. H.-C. W. and M. A. L. M. would like to thank the NHR Centre PC2 for providing computing time on the Noctua 2 supercomputers.

References

1 H.-D. Liu, X.-P. Fu, Z.-G. Fu, H.-Y. Lu and P. Zhang, New-record-Tc and three-gap 2D superconductors with electronic and phononic topology: KB_2C_2, *arXiv*, 2024, preprint, arXiv:2408.12242, DOI: 10.48550/arXiv.2408.12242.

2 R. Brüning, J. Bedow, R. L. Conte, K. von Bergmann, D. K. Morr and R. Wiesendanger, The noncollinear path to topological superconductivity, *arXiv*, 2024, preprint, arXiv:2405.14673, DOI: 10.48550/arXiv.2405.14673.

3 A. Arora, J. B. Curtis and P. Narang, Quantum geometry induced microwave enhancement of flat band superconductivity, *arXiv*, 2024, preprint, arXiv:2411.03437, DOI: 10.48550/arXiv.2411.03437.

4 G. Feraco, W. Boubaker, P. Rudolf and A. GrubišićČabo, Exotic quantum phenomena in twisted bilayer graphene, *arXiv*, 2024, preprint, arXiv:2411.00854, DOI: 10.48550/arXiv.2411.00854.

5 J. Camps, O. Crawford, G. P. Gehér, A. V. Gramolin, M. P. Stafford and M. Turner, Leakage mobility in superconducting qubits as a leakage reduction unit, *arXiv*, 2024, preprint, arXiv:2406.04083, DOI: 10.48550/arXiv.2406.04083.

6 L. Caune, L. Skoric, N. S. Blunt, A. Ruban, J. Mc-Daniel, J. A. Valery, A. D. Patterson, A. V. Gramolin, J. Majaniemi, K. M. Barnes, T. Bialas, O. Buğdaycı, O. Crawford, G. P. Gehér, H. Krovi, E. Matekole, C. Topal, S. Poletto, M. Bryant, K. Snyder, N. I. Gillespie, G. Jones, K. Johar, E. T. Campbell and A. D. Hill, Demonstrating real-time and low-latency quantum error correction with superconducting qubits, *arXiv*, 2024, preprint, arXiv:2410.05202, DOI: 10.48550/arXiv.2410.05202.

7 Q. Zhang, M. S. Hossain, B. Casas, W. Zheng, Z.-J. Cheng, Z. Lai, Y.-H. Tu, G. Chang, Y. Yao, S. Li, Y.-X. Jiang, S. Mardanya, T.-R. Chang, J.-Y. You, Y.-P. Feng, G. Cheng, J.-X. Yin, N. Shumiya, T. A. Cochran, X. P. Yang, M. Litskevich, N. Yao, K. Watanabe, T. Taniguchi, H. Zhang, L. Balicas and M. Z. Hasan, Ultrahigh supercurrent density in a two-dimensional topological material, *Phys. Rev. Mater.*, 2023, **7**, L071801.

8 R. F. Frindt, Superconductivity in ultrathin $NbSe_2$ layers, *Phys. Rev. Lett.*, 1972, **28**, 299–301.

9 I. Guillamón, H. Suderow, S. Vieira, L. Cario, P. Diener and P. Rodière, Superconducting density of states and vortex cores of 2H-NbS2, *Phys. Rev. Lett.*, 2008, **101**, 166407.

10 L. J. Li, E. C. T. O'Farrell, K. P. Loh, G. Eda, B. Özyilmaz and A. H. Castro Neto, Controlling many-body states by the electric-field effect in a two-dimensional material, *Nature*, 2015, **529**, 185–189.

11 E. Navarro-Moratalla, J. O. Island, S. Mañas-Valero, E. Pinilla-Cienfuegos, A. Castellanos-Gomez, J. Quereda, G. Rubio-Bollinger, L. Chirolli, J. A. Silva- Guillén, N. Agraït, G. A. Steele, F. Guinea, H. S. J. van der Zant and E. Coronado, Enhanced superconductivity in atomically thin TaS_2, *Nat. Commun.*, 2016, **7**, 11043.

12 J. M. Lu, O. Zheliuk, I. Leermakers, N. F. Q. Yuan, U. Zeitler, K. T. Law and J. T. Ye, Evidence for two-dimensional Ising superconductivity in gated MoS_2, *Science*, 2015, **350**, 1353–1357.

13 D. Qiu, C. Gong, S. Wang, M. Zhang, C. Yang, X. Wang and J. Xiong, Recent advances in 2D superconductors, *Adv. Mater.*, 2021, **33**, 2006124.

14 M. Calandra and F. Mauri, Charge-density wave and superconducting dome in TiSe2 from electron-phonon interaction, *Phys. Rev. Lett.*, 2011, **106**, 196406.

15 X. Xi, L. Zhao, Z. Wang, H. Berger, L. Forró, J. Shan and K. F. Mak, Strongly enhanced charge-densitywave order in monolayer $NbSe_2$, *Nat. Nanotechnol.*, 2015, **10**, 765–769.

16 D. Möckli and M. Khodas, Robust parity-mixed superconductivity in disordered monolayer transition metal dichalcogenides, *Phys. Rev. B*, 2018, **98**, 144518.

17 X. Xi, Z. Wang, W. Zhao, J.-H. Park, K. T. Law, H. Berger, L. Forró, J. Shan and K. F. Mak, Ising pairing in superconducting NbSe2 atomic layers, *Nat. Phys.*, 2015, **12**, 139–143.

18 W. Li, J. Huang, X. Li, S. Zhao, J. Lu, Z. V. Han and H. Wang, Recent progresses in two-dimensional Ising superconductivity, *Mater. Today Phys.*, 2021, **21**, 100504.

19 K. Ghosh, H. Rahaman and P. Bhattacharyya, Prediction and implementation of graphene and other twodimensional material based superconductors: A review, *IEEE Trans. Appl. Supercond.*, 2020, **30**, 1–9.

20 C.-W. Chen, J. Choe and E. Morosan, Charge density waves in strongly correlated electron systems, *Rep. Prog. Phys.*, 2016, **79**, 084505.

21 D. Wickramaratne, S. Khmelevskyi, D. F. Agterberg and I. Mazin, Ising superconductivity and magnetism in $NbSe_2$, *Phys. Rev. X*, 2020, **10**, 041003.

22 C. Heil, S. Poncé, H. Lambert, M. Schlipf, E. R. Margine and F. Giustino, Origin of superconductivity and latent charge density wave in NbS_2, *Phys. Rev. Lett.*, 2017, **119**, 087003.

23 N. F. Hinsche and K. S. Thygesen, Electron–phonon interaction and transport properties of metallic bulk and monolayer transition metal dichalcogenide TaS_2, *2D Mater.*, 2017, **5**, 015009.

24 Y. Ge and A. Y. Liu, Phonon-mediated superconductivity in electron-doped single-layer MoS_2: A firstprinciples prediction, *Phys. Rev. B*, 2013, **87**, 241408(R).

25 C.-S. Lian, Interplay of charge ordering and superconductivity in two-dimensional 2H group V transitionmetal dichalcogenides, *Phys. Rev. B*, 2023, **107**, 045431.

26 R. Szcześniak, A. P. Durajski and M. W. Jarosik, Strong-coupling superconductivity induced by calcium intercalation in bilayer transition-metal dichalcogenides, *Front. Phys.*, 2017, **13**, 137401.

27 B.-T. Wang, P.-F. Liu, T. Bo, W. Yin, O. Eriksson, J. Zhao and F. Wang, Superconductivity in twodimensional phosphorus carbide (β0-PC), *Phys. Chem. Chem. Phys.*, 2018, **20**, 12362–12367.
28 D.-L. Nguyen, C.-R. Hsing and C.-M. Wei, Theoretical prediction of superconductivity in monolayer CoO_2, *Nanoscale*, 2019, **11**, 17052.
29 J. Liu, H. Wang, X. Shi and X. Zhang, Prediction of superconductivity in a series of tetragonal transition metal dichalcogenides, *Mater. Horiz.*, 2024, **11**, 2694–2700.
30 Y. Cao, V. Fatemi, A. Demir, S. Fang, S. L. Tomarken, J. Y. Luo, J. D. Sanchez-Yamagishi, K. Watanabe, T. Taniguchi, E. Kaxiras, R. C. Ashoori and P. Jarillo- Herrero, Correlated insulator behaviour at half-filling in magic-angle graphene superlattices, *Nature*, 2018, **556**, 80–84.
31 Y. Cao, V. Fatemi, S. Fang, K. Watanabe, T. Taniguchi, E. Kaxiras and P. Jarillo-Herrero, Unconventional superconductivity in magic-angle graphene superlattices, *Nature*, 2018, **556**, 43–50.
32 T. Löthman and A. M. Black-Schaffer, Defects in the d + id-wave superconducting state in heavily doped graphene, *Phys. Rev. B*, 2014, **90**, 224504.
33 G. Profeta, M. Calandra and F. Mauri, Phononmediated superconductivity in graphene by lithium deposition, *Nat. Phys.*, 2012, **8**, 131–134.
34 H.-Y. Lu, Y. Yang, L. Hao, W.-S. Wang, L. Geng, M. Zheng, Y. Li, N. Jiao, P. Zhang and C. S. Ting, Phonon-mediated superconductivity in aluminumdeposited graphene AlC8, *Phys. Rev. B*, 2020, **101**, 214514.
35 R. Liu, J. Lu, H. Chen, X. Zhao, G. Hu, X. Yuan and J. Ren, Prediction of π-electrons mediated hightemperature superconductivity in monolayer $LiC1_2$, *J. Phys.: Condens. Matter*, 2023, **35**, 144001.
36 N. H. Shimada, E. Minamitani and S. Watanabe, Theoretical prediction of phonon-mediated superconductivity with $T_c \approx 25$ K in Li-intercalated hexagonal boron nitride bilayer, *Appl. Phys. Express*, 2017, **10**, 093101.
37 Y.-T. Kang, C. Lu, F. Yang and D.-X. Yao, Singleorbital realization of high-temperature s± superconductivity in the square-octagon lattice, *Phys. Rev. B*, 2019, **99**, 184506.
38 J. Li, S. Jin, F. Yang and D.-X. Yao, Electronic structure, magnetism, and high-temperature superconductivity in multilayer octagraphene and octagraphite, *Phys. Rev. B*, 2020, **102**, 174509.
39 J. Ye, J. Li, D. Zhong and D.-X. Yao, Possible superconductivity in biphenylene, *Chin. Phys. Lett.*, 2023, **40**, 077401.
40 Q. Gu, D. Xing and J. Sun, Superconducting singlelayer T-graphene and novel synthesis routes, *Chin. Phys. Lett.*, 2019, **36**, 097401.
41 N. Lu, Z. Li and J. Yang, Electronic structure engineering via on-plane chemical functionalization: A comparison study on two-dimensional polysilane and graphane, *J. Phys. Chem. C*, 2009, **113**, 16741–16746.
42 D. C. Elias, R. R. Nair, T. M. G. Mohiuddin, S. V. Morozov, P. Blake, M. P. Halsall, A. C. Ferrari, D. W. Boukhvalov, M. I. Katsnelson, A. K. Geim and K. S. Novoselov, Control of graphene's properties by reversible hydrogenation: Evidence for graphane, *Science*, 2009, **323**, 610–613.
43 C. Zhou, S. Chen, J. Lou, J. Wang, Q. Yang, C. Liu, D. Huang and T. Zhu, Graphene's cousin: the present and future of graphane, *Nanoscale Res. Lett.*, 2014, **9**, 26.
44 M. Bonfanti, S. Achilli and R. Martinazzo, Sticking of atomic hydrogen on graphene, *J. Phys.: Condens. Matter*, 2018, **30**, 283002.
45 G. Savini, A. C. Ferrari and F. Giustino, Firstprinciples prediction of doped graphane as a hightemperature electron-phonon superconductor, *Phys. Rev. Lett.*, 2010, **105**, 037002.
46 J. Noffsinger and M. L. Cohen, Superconductivity in monolayer Pb on Si(111) from first principles, *Solid State Commun.*, 2011, **151**, 421–424.
47 W. Wan, Y. Ge, F. Yang and Y. Yao, Phononmediated superconductivity in silicene predicted by first-principles density functional calculations, *Europhys. Lett.*, 2013, **104**, 36001.
48 D. F. Shao, W. J. Lu, H. Y. Lv and Y. P. Sun, Electrondoped phosphorene: A potential monolayer superconductor, *Europhys. Lett.*, 2014, **108**, 67004.
49 J. Chen, Y. Ge, W. Zhou, M. Peng, J. Pan and F. Ouyang, Superconductivity in Li-intercalated bilayer arsenene and hole-doped monolayer arsenene: a firstprinciples prediction, *J. Phys.: Condens. Matter*, 2018, **30**, 245701.
50 I. Serifi, N. B. J. Kanga, L. B. Drissi and E. H. Saidi, Electron-phonon contribution in aluminene: Su perconductive and transport properties, *Superlattices Microstruct.*, 2021, **151**, 106822.
51 M. Petrov, J. Bekaert and M. V. Milošević, Superconductivity in gallenene, *2D Mater.*, 2021, **8**, 035056.
52 A. V. Lugovskoi, M. I. Katsnelson and A. N. Rudenko, Electron-phonon properties, structural stability, and superconductivity of doped antimonene, *Phys. Rev. B*, 2019, **99**, 064513.
53 M. Gao, Q.-Z. Li, X.-W. Yan and J. Wang, Prediction of phonon-mediated superconductivity in borophene, *Phys. Rev. B*, 2017, **95**, 024505.
54 E. S. Penev, A. Kutana and B. I. Yakobson, Can two-dimensional boron superconduct?, *Nano Lett.*, 2016, **16**, 2522–2526.
55 Y. Zhao, S. Zeng and J. Ni, Superconductivity in twodimensional boron allotropes, *Phys. Rev. B*, 2016, **93**, 014502.
56 L. Yang, Y.-P. Li, H.-D. Liu, N. Jiao, M.-Y. Ni, H.-Y. Lu, P. Zhang and C. S. Ting, Theoretical prediction of superconductivity in boron kagome monolayer: MB3 (M = Be, Ca, Sr) and the hydrogenated CaB_3, *Chin. Phys. Lett.*, 2023, **40**, 017402.
57 S.-Y. Xie, X.-B. Li, W. Q. Tian, N.-K. Chen, Y. Wang, S. Zhang and H.-B. Sun, A novel two-dimensional MgB_6 crystal: metal-layer stabilized boron kagome lattice, *Phys. Chem. Chem. Phys.*, 2015, **17**, 1093–1098.
58 T. Bo, P.-F. Liu, L. Yan and B.-T. Wang, Electronphonon coupling superconductivity in two-dimensional orthorhombic MB6 (M = Mg,Ca,Ti,Y) and hexagonal MB6 (M = Mg,Ca,Sc,Ti), *Phys. Rev. Mater.*, 2020, **4**, 114802.

59 C. Wu, H. Wang, J. Zhang, G. Gou, B. Pan and J. Li, Lithium–boron (Li–B) monolayers: First-principles cluster expansion and possible two-dimensional superconductivity, *ACS Appl. Mater. Interfaces*, 2016, **8**, 2526–2532.
60 L. Yan, T. Bo, P.-F. Liu, L. Zhou, J. Zhang, M.-H. Tang, Y.-G. Xiao and B.-T. Wang, Superconductivity in predicted two dimensional XB6 (X = Ga, In), *J. Mater. Chem. C*, 2020, **8**, 1704–1714.
61 B. Song, Y. Zhou, H.-M. Yang, J.-H. Liao, L.-M. Yang, X.-B. Yang and E. Ganz, Two-dimensional anti-van't hoff/le bel array AlB6 with high stability, unique motif, triple Dirac cones, and superconductivity, *J. Am. Chem. Soc.*, 2019, **141**, 3630–3640.
62 L. Yan, T. Bo, W. Zhang, P.-F. Liu, Z. Lu, Y.-G. Xiao, M.-H. Tang and B.-T. Wang, Novel structures of twodimensional tungsten boride and their superconductivity, *Phys. Chem. Chem. Phys.*, 2019, **21**, 15327–15338.
63 L. Yan, T. Bo, P.-F. Liu, B.-T. Wang, Y.-G. Xiao and M.-H. Tang, Prediction of phonon-mediated superconductivity in two-dimensional Mo_2B_2, *J. Mater. Chem. C*, 2019, **7**, 2589.
64 L. Wang, M. Liu, J. Li, R. Li, H. Ma and X.-Q. Chen, Topological nodal line and superconductivity of highly thermally stable two-dimensional TiB_4, *Phys. Rev. B*, 2021, **104**, 195123.
65 S. Chen, H. Xie, D. Xu, J. Chen, B. Cao, M. Liang, Y. Sun, X. Gai, X. Wang, M. Yang, M. Zhang, D. Duan, D. Li and F. Tian, Superconductivity of cubic MB6 (M = Na, K, Rb, Cs), *J. Chem. Phys.*, 2024, **160**, 044702.
66 M. U. Farooq, A. Hashmi, I. Khan and J. Hong, Superconductivity in two-dimensional ferromagnetic MnB, *Sci. Rep.*, 2017, **7**, 17101.
67 Z. Qu, F. Han, T. Yu, M. Xu, Y. Li and G. Yang, Boron kagome-layer induced intrinsic superconductivity in a MnB_3 monolayer with a high critical temperature, *Phys. Rev. B*, 2020, **102**, 075431.
68 Y.-L. Han, Y.-P. Li, L. Yang, H.-D. Liu, N. Jiao, B.-T. Wang, H.-Y. Lu and P. Zhang, High-temperature superconductivity in two-dimensional hydrogenated titanium diboride: $Ti_2B_2H_4$, *Mater. Today Phys.*, 2023, **30**, 100954.
69 H. Wang, C. Pan, S.-Y. Wang, H. Jiang, Y.-C. Zhao, Y.-H. Su, G.-H. Zhong and C. Zhang, Hydrogenation as a source of superconductivity in two-dimensional TiB_2, *Int. J. Mod. Phys. C*, 2021, **32**, 2150057.
70 J. Dai, Z. Li, J. Yang and J. Hou, A first-principles prediction of two-dimensional superconductivity in pristine B_2C single layers, *Nanoscale*, 2012, **4**, 3032.
71 S. Singh, A. H. Romero, J. D. Mella, V. Eremeev, E. Muñoz, A. N. Alexandrova, K. M. Rabe, D. Vanderbilt and F. Muñoz, High-temperature phonon-mediated superconductivity in monolayer Mg_2B4C_2, *npj Quantum Mater.*, 2022, **7**, 37.
72 Y. Zhang, J. Chen, J. Hao, M. Xu and Y. Li, Conventional high-temperature superconductivity in σ-band driven metallized two-dimensional metal borocarbides, *Phys. Rev. B*, 2024, **110**, 064513.
73 L.-B. Meng, M. J. Zhou, Y. J. Zhang and S. Ni, Intrinsic phonon-mediated superconductivity in graphenelike BSi lattice, *J. Phys.: Condens. Matter*, 2019, **31**, 345401.
74 I. Serifi, N. B.-J. Kanga, L. B. Drissi, A. Kara and E. H. Saidi, Electron–phonon superconductivity in boronbased chalcogenide (X = S, Se) monolayers, *Ann. Phys.*, 2023, **535**, 2200539.
75 H.-D. Liu, J.-G. Si, N. Jiao, Y.-L. Han, M.-M. Zheng, H.-Y. Lu, B.-T. Wang and P. Zhang, Superconducting two-dimensional penta materials, *Mater. Today Phys.*, 2024, **40**, 101305.
76 B.-T. Liu, Y.-P. Li and H.-Y. Lu, Phonon-mediated superconductivity in two-dimensional MBP (M = Li, Na,Ti), *J. Low Temp. Phys.*, 2022, **210**, 129.
77 H. Li, J. Min, Z. Yang, Z. Wang, S. Pan and A. R. Oganov, Prediction of novel van der Waals boron oxides with superior deep-ultraviolet nonlinear optical performance, *Angew. Chem., Int. Ed.*, 2021, **60**, 10791–10797.
78 L. Yan, P.-F. Liu, H. Li, Y. Tang, J. He, X. Huang, B.-T. Wang and L. Zhou, Theoretical dissection of superconductivity in two-dimensional honeycomb borophene oxide B_2O crystal with a high stability, *npj Comput. Mater.*, 2020, **6**, 94.
79 D. Campi, S. Kumari and N. Marzari, Prediction of phonon-mediated superconductivity with high critical temperature in the two-dimensional topological semimetal W_2N_3, *Nano Lett.*, 2021, **21**, 3435–3442.
80 Q. Wu, J.-J. Zhang, P. Hao, Z. Ji, S. Dong, C. Ling, Q. Chen and J. Wang, Versatile titanium silicide monolayers with prominent ferromagnetic, catalytic, and superconducting properties: Theoretical prediction, *J. Phys. Chem. Lett.*, 2016, **7**, 3723–3729.
81 W. Jin, J. Zuo, J. Pang, J. Yang, X. Yu, H. Zhong, X. Kuang and C. Lu, Two-dimensional $MoSi_2N_4$ family: Progress and perspectives form theory, *J. Phys. Chem. Lett.*, 2024, **15**, 10284–10294.
82 X. Zhang, Y. Zhou, B. Cui, M. Zhao and F. Liu, Theoretical discovery of a superconducting two-dimensional metal–organic framework, *Nano Lett.*, 2017, **17**, 6166–6170.
83 J. Lei, A. Kutana and B. I. Yakobson, Predicting stable phase monolayer Mo_2C (MXene), a superconductor with chemically-tunable critical temperature, *J. Mater. Chem. C*, 2017, **5**, 3438–3444.
84 J. Bekaert, C. Sevik and M. V. Milošević, Firstprinciples exploration of superconductivity in MXenes, *Nanoscale*, 2020, **12**, 17354–17361.
85 A. N. Tatan and O. Sugino, Exploring functionalized Zr_2N and Sc_2N MXenes as superconducting candidates with ab initio calculations, arXiv, *arxiv.*, 2024, **2409**, 12052.
86 Z. S. Pereira, G. M. Faccin and E. Z. da Silva, Straininduced multigap superconductivity in electrene Mo2N: a first principles study, *Nanoscale*, 2022, **14**, 8594–8600.
87 J.-J. Zhang and S. Dong, Superconductivity of monolayer Mo_2C: The key role of functional groups, *J. Chem. Phys.*, 2017, **146**, 034705.
88 N. Jiao, H.-D. Liu, L. Yang, Y.-P. Li, M. Zheng, H.-Y. Lu and P. Zhang, Hydrogenation-induced high-temperature superconductivity in two-dimensional molybdenum carbide Mo2C3, *Europhys. Lett.*, 2022, **138**, 46002.
89 J. Bekaert, C. Sevik and M. V. Milošević, Enhancing superconductivity in MXenes through hydrogenation, *Nanoscale*, 2022, **14**, 9918–9924.

90 A. Jain, S. P. Ong, G. Hautier, W. Chen, W. D. Richards, S. Dacek, S. Cholia, D. Gunter, D. Skinner, G. Ceder and K. A. Persson, Commentary: The materials project: A materials genome approach to accelerating materials innovation, *APL Mater.*, 2013, **1**, 011002.

91 S. Kirklin, J. E. Saal, B. Meredig, A. Thompson, J. W. Doak, M. Aykol, S. Rühl and C. Wolverton, The open quantum materials database (OQMD): assessing the accuracy of DFT formation energies, *npj Comput. Mater.*, 2015, **1**, 15010.

92 S. Curtarolo, W. Setyawan, G. L. Hart, M. Jahnatek, R. V. Chepulskii, R. H. Taylor, S. Wang, J. Xue, K. Yang, O. Levy, M. J. Mehl, H. T. Stokes, D. O. Demchenko and D. Morgan, Aflow: An automatic framework for high-throughput materials discovery, *Comput. Mater. Sci.*, 2012, **58**, 218–226.

93 M. N. Gjerding, A. Taghizadeh, A. Rasmussen, S. Ali, F. Bertoldo, T. Deilmann, N. R. Knøsgaard, M. Kruse, A. H. Larsen, S. Manti, T. G. Pedersen, U. Petralanda, T. Skovhus, M. K. Svendsen, J. J. Mortensen, T. Olsen and K. S. Thygesen, Recent progress of the computational 2D materials database (C_2DB), *2D Mater.*, 2021, **8**, 044002.

94 D. Campi, N. Mounet, M. Gibertini, G. Pizzi and N. Marzari, Expansion of the materials cloud 2d database, *ACS Nano*, 2023, **17**, 11268–11278.

95 N. Mounet, M. Gibertini, P. Schwaller, D. Campi, A. Merkys, A. Marrazzo, T. Sohier, I. E. Castelli, A. Cepellotti, G. Pizzi and N. Marzari, Two-dimensional materials from high-throughput computational exfoliation of experimentally known compounds, *Nat. Nanotechnol.*, 2018, **13**, 246–252.

96 H.-C. Wang, J. Schmidt, M. A. L. Marques, L. Wirtz and A. H. Romero, Symmetry-based computational search for novel binary and ternary 2D materials, *2D Mater.*, 2023, **10**, 035007.

97 J. Schmidt, M. R. G. Marques, S. Botti and M. A. L. Marques, Recent advances and applications of machine learning in solid-state materials science, *npj Comput. Mater.*, 2019, **5**, 83.

98 K. Choudhary and K. Garrity, Designing high-TC superconductors with BCS-inspired screening, density functional theory, and deep-learning, *npj Comput. Mater.*, 2022, **8**, 244.

99 N. K. Nepal and L.-L. Wang, Machine-learning guided search for phonon-mediated superconductivity in boron and carbon compounds, 2024.

100 H. Tran and T. N. Vu, Machine-learning approach for discovery of conventional superconductors, *Phys. Rev. Mater.*, 2023, **7**, 054805.

101 T. F. T. Cerqueira, A. Sanna and M. A. L. Marques, Sampling the materials space for conventional superconducting compounds, *Adv. Mater.*, 2023, **36**, 2307085.

102 K. Dolui, L. J. Conway, C. Heil, T. A. Strobel, R. P. Prasankumar and C. J. Pickard, Feasible route to high-temperature ambient-pressure hydride superconductivity, *Phys. Rev. Lett.*, 2024, **132**, 166001.

103 A. Sanna, T. F. T. Cerqueira, Y.-W. Fang, I. Errea, A. Ludwig and M. A. L. Marques, Prediction of ambient pressure conventional superconductivity above 80 K in hydride compounds, *npj Comput. Mater.*, 2024, **10**, 44.

104 D. Wines, K. Choudhary, A. J. Biacchi, K. F. Garrity and F. Tavazza, High-throughput DFT-based discovery of next generation two-dimensional (2D) superconductors, *Nano Lett.*, 2023, **23**, 969–978.

105 D. Wines, R. Gurunathan, K. F. Garrity, B. DeCost, A. J. Biacchi, F. Tavazza and K. Choudhary, Recent progress in the jarvis infrastructure for next-generation data-driven materials design, *Appl. Phys. Rev.*, 2023, **10**, 041302.

106 P. B. Allen and R. C. Dynes, Transition temperature of strong-coupled superconductors reanalyzed, *Phys. Rev. B*, 1975, **12**, 905.

107 W. L. McMillan, Transition temperature of strongcoupled superconductors, *Phys. Rev.*, 1968, **167**, 331.

108 R. Dynes, Mcmillan's equation and the tc of superconductors, *Solid State Commun.*, 1972, **10**, 615–618.

109 P. Virtanen, R. Gommers, T. E. Oliphant, M. Haberland, T. Reddy, D. Cournapeau, E. Burovski, P. Peterson, W. Weckesser, J. Bright, S. J. van der Walt, M. Brett, J. Wilson, K. J. Millman, N. Mayorov, A. R. J. Nelson, E. Jones, R. Kern, E. Larson, C. J. Carey, İ. Polat, Y. Feng, E. W. Moore, J. VanderPlas, D. Laxalde, J. Perktold, R. Cimrman, I. Henriksen, E. A. Quintero, C. R. Harris, A. M. Archibald, A. H. Ribeiro, F. Pedregosa and P. van Mulbregt, and SciPy 1.0 Contributors, SciPy 1.0: Fundamental Algorithms for Scientific Computing in Python, *Nat. Methods*, 2020, **17**, 261.

110 N. W. Ashcroft, Metallic hydrogen: A high-temperature superconductor?, *Phys. Rev. Lett.*, 1968, **21**, 1748–1749.

111 E. Wigner and H. B. Huntington, On the possibility of a metallic modification of hydrogen, *J. Chem. Phys.*, 1935, **3**, 764–770.

112 P. Giannozzi, S. Baroni, N. Bonini, M. Calandra, R. Car, C. Cavazzoni, D. Ceresoli, G. L. Chiarotti, M. Cococcioni, I. Dabo, A. Dal Corso, S. de Gironcoli, S. Fabris, G. Fratesi, R. Gebauer, U. Gerstmann, C. Gougoussis, A. Kokalj, M. Lazzeri, L. Martin-Samos, N. Marzari, F. Mauri, R. Mazzarello, S. Paolini, A. Pasquarello, L. Paulatto, C. Sbraccia, S. Scandolo, G. Sclauzero, A. P. Seitsonen, A. Smogunov, P. Umari and R. M. Wentzcovitch, Quantum espresso: a modular and open-source software project for quantum simulations of materials, *J. Phys.: Condens. Matter*, 2009, **21**, 395502.

113 P. Giannozzi, O. Andreussi, T. Brumme, O. Bunau, M. Buongiorno Nardelli, M. Calandra, R. Car, C. Cavazzoni, D. Ceresoli, M. Cococcioni, N. Colonna, I. Carnimeo, A. Dal Corso, S. de Gironcoli, P. Delugas, R. A. DiStasio, A. Ferretti, A. Floris, G. Fratesi, G. Fugallo, R. Gebauer, U. Gerstmann, F. Giustino, T. Gorni, J. Jia, M. Kawamura, H.-Y. Ko, A. Kokalj, E. Küçükbenli, M. Lazzeri, M. Marsili, N. Marzari, F. Mauri, N. L. Nguyen, H.-V. Nguyen, A. Otero-dela Roza, L. Paulatto, S. Poncé, D. Rocca, R. Sabatini, B. Santra, M. Schlipf, A. P. Seitsonen, A. Smogunov, I. Timrov, T. Thonhauser, P. Umari, N. Vast, X. Wu and S. Baroni, Advanced capabilities for materials modelling with quantum espresso, *J. Phys.: Condens. Matter*, 2017, **29**, 465901.

114 J. P. Perdew, A. Ruzsinszky, G. I. Csonka, O. A. Vydrov, G. E. Scuseria, L. A. Constantin, X. Zhou and K. Burke,

Restoring the density-gradient expansion for exchange in solids and surfaces, *Phys. Rev. Lett.*, 2008, **100**, 136406.
115 M. van Setten, M. Giantomassi, E. Bousquet, M. Verstraete, D. Hamann, X. Gonze and G.-M. Rignanese, The pseudodojo: Training and grading a 85 element optimized norm-conserving pseudopotential table, *Comput. Phys. Commun.*, 2018, **226**, 39–54.
116 T. Sohier, M. Calandra and F. Mauri, Density functional perturbation theory for gated two-dimensional heterostructures: Theoretical developments and application to flexural phonons in graphene, *Phys. Rev. B*, 2017, **96**, 075448.
117 K. Choudhary and B. DeCost, Atomistic line graph neural network for improved materials property predictions, *npj Comput. Mater.*, 2021, **7**, 185.